International Journal of Mass Spectrometry 309 (2012) 118–128

Contents lists available at SciVerse ScienceDirect

International Journal of Mass Spectrometry

journal homepage: www.elsevier.com/locate/ijms

Absolute photoionization cross-sections of some combustion intermediates

Bin Yang[a], Juan Wang[a], Terrill A. Cool[a,*], Nils Hansen[b], Scott Skeen[b], David L. Osborn[b]

[a] School of Applied and Engineering Physics, Cornell University, Ithaca, NY 14853, USA
[b] Combustion Research Facility, Sandia National Laboratories, Livermore, CA 94551, USA

ARTICLE INFO

Article history:
Received 12 August 2011
Received in revised form 8 September 2011
Accepted 8 September 2011
Available online 16 September 2011

Keywords:
Photoionization cross-sections
Photodissociation
Photoionization mass spectrometry (PIMS)
Combustion chemistry
Oxygenates
Nitrogenous compounds

ABSTRACT

Near-threshold absolute photoionization and dissociative photoionization cross-sections for photon energies from 9.7 to 11.75 eV are presented for 30 combustion intermediates including hydrocarbons, oxygenates and nitrogenous compounds (trans-2-butene, 2-methyl-1-butene, 3-methyl-1-butene, 2-methyl-2-butene, trans-2-hexene, 1-hexene, allene, 1,3-butadiene, 1,3-pentadiene, 1,4-pentadiene, 3-methyl-1,2-butadiene, 1,5-hexadiene, isobutane, methylcyclohexane, furan, 2,3-dihydrofuran, 2,5-dihydrofuran, 2-methyltetrahydrofuran, tetrahydropyran, n-butanal, isobutanal, 2-butenal, 3-methyl-2-butenal, ketene, allyl alcohol, methyl vinyl ketone, dimethoxymethane, methylamine, ethylamine, piperidine). Because allene is one of the most important intermediates in hydrocarbon combustion and pyrolysis processes, very accurate cross-sections for allene are desired to enable the measurement of its mole fractions in flames and to determine relative concentration ratios of allene to its isomer propyne. The cross-sections for allene have thus been re-measured with high precision using an apparatus of improved signal/noise ratio. Furthermore, these allene cross-sections yield accurate previously unmeasured cross-sections for ketene, another key combustion intermediate.

1. Introduction

Benefiting from the development of intense vacuum ultraviolet (VUV) light sources, including synchrotrons, discharge lamps and VUV lasers, single-photon ionization mass spectrometry (PIMS) has recently become increasingly popular for characterizing complex gas-mixtures in chemically reacting systems in atmospheric chemistry, aerosol chemistry, laser-initiated chemical kinetics, low-pressure flames and related processes [1–7]. These PIMS measurements utilize single VUV radiation to photoionize reaction intermediates, products, and photofragments, which are mass-selected and detected. PIMS usually yields substantially less fragmentation upon ionization than electron ionization mass spectrometry (EIMS), and it is particularly useful for those species which cannot be detected by alternative methods such as resonance-enhanced multiphoton ionization or laser-induced fluorescence because of a lack of suitable excited states of the neutral.

Absolute photoionization cross-sections obtained with VUV PIMS are necessary to quantify the concentrations of the species of interest. Because photoionization of a polyatomic species can often result in dissociative ionization within 1–2 eV of the adiabatic ionization energy of the parent molecule, these contributions to the total photoionization cross-sections must be determined. To avoid the interference between the parent ions of a given mass-to-charge (m/z) and ion fragments with the same m/z derived from other bigger species in a complex system, an accurate determination of mass-resolved partial photoionization cross-sections for parent and dissociative ions are highly desirable for all chemical species probed. Take flame chemistry studies for example; mass-resolved partial cross-sections for combustion intermediates enable species identification through photoionization efficiency (PIE) measurements [3,8,9] and facilitate quantitative determination of mole fractions [10]. Unfortunately, the established photoionization cross section database for hundreds of flames species is far from complete.

Measurement of absolute cross-sections for stable species has been carried out by several different methods. A dual beam single ion chamber [11–14] and a double ion chamber [15–25] are often used to determine the total photoionization cross section through the measurement of the absolute photoabsorption cross section and a determination of the ionization quantum yield. Once the absolute photoionization cross section for one species is known, the absolute photoionization cross-sections for other species can be determined by relative measurements of both species [3,26–34]. Our group has recently determined the absolute photoionization cross-sections for a number of stable combustion intermediates by making relative measurements with respect to propene [3,27,28,35]. More recently, Zhou et al. and Xie et al. [29–32] have measured photoionization cross-sections for a series of compounds with binary-liquid-mixture methods using

* Corresponding author. Tel.: +1 607 2554191; fax: +1 607 2557658.
E-mail address: tac13@cornell.edu (T.A. Cool).

1387-3806/$ – see front matter © 2011 Elsevier B.V. All rights reserved.
doi:10.1016/j.ijms.2011.09.006

cross-sections for benzene as calibration standards. In addition, absolute photoionization cross-sections for free radicals including methyl [36,37], ethyl [38], vinyl [39], propargyl [39], allyl [40], 2-propenyl [40,41], isopropyl [42], phenyl [43], and formyl [44] have been determined using several different approaches.

In this paper, we present measurements of total and mass-resolved partial photoionization and photodissociation cross-sections for 30 reaction intermediates for photon energies ranging from their respective ionization thresholds up to 11.75 eV. Of particular interest, we present new high accuracy measurements of allene cross-sections using an apparatus of improved signal/noise ratio [3]. These allene cross-sections enable the determination of accurate, previously unmeasured cross-sections for ketene, another key combustion intermediate. The experimental results contribute to a fast growing database of photoionization cross-sections of importance for studies of gas phase chemistry with PIMS.

2. Experiments

The experiments described in this paper are performed using a molecular-beam time-of-flight photoionization mass spectrometer. A detailed description of the experimental apparatus and measurement procedures have been provided elsewhere [35]. Briefly, the apparatus consists of a low pressure (ca. 15 Torr) stainless steel sample reservoir, a two-stage differentially pumped molecular beam sampling system, and a 1.3-m linear time-of-flight mass spectrometer (TOFMS) with a mass resolution $m/\Delta m = 400$. It is coupled to a 3-m monochromator used to disperse synchrotron radiation at the Advanced Light Source (ALS) of the Lawrence Berkeley National Laboratory [45]. The dispersed photon beam is tunable over the useful range from 8 to 17 eV with a typical energy resolution of 40 meV (fwhm) and photon current of 5×10^{13} photons/s. As in previous studies [35], photoionization cross-sections for target species are determined by calibration of photo-ion signals from the target species against those of propene as a calibration standard with accurately measured photoionization cross-sections over the photon energy range from 9.7 to 11.75 eV [13]. Binary mixtures of a given target molecule with propene are prepared in a 3.8 l stainless steel sample cylinder with a Teflon coated inner surface. Nominal sample mixture compositions consist of 15 Torr each of the target molecule and propene to which 2300 Torr of argon diluent is added. The samples are allowed to mix for at least 8 h and then are introduced as a cold flow to the sample reservoir at a flow rate of 0.12 slm (standard liters per minute) along with a second flow of argon at 0.25 slm. The gas mixture passing from the reservoir with a pressure of 15 Torr expands into the ionization region, where it is crossed by the dispersed VUV light from the monochromator.

Photo-ions extracted by pulse-gating a repeller plate are propelled along the flight tube of the TOFMS and detected by a microchannel plate. Ion counts as a function of ion flight times (15,008 channels of 2 ns bin width) are recorded for 5×10^5 to 2×10^6 sweeps of a multichannel scaler (Fast ComTek P7886). The resulting mass spectra (ion signal *vs* m/z), obtained from accumulated ion counts integrated over each mass peak, are corrected for background signals and overlapping contributions from ^{13}C isotopes and finally normalized by the photon current to yield photoionization efficiencies as a function of photon energy (PIE spectra) for both the target molecule and the propene calibration standard.

Absolute photoionization cross-sections for parent ions of the target species are obtained from the PIE spectra for the parent ion and propene with the relationship [35]

$$\sigma_T(E) = \frac{\sigma_S(E)[S_T(E)P_S/S_S(E)P_T]}{R_T/R_S} \quad (1)$$

Here $\sigma_T(E)$ and $\sigma_S(E)$ are the respective energy-dependent photoionization cross-sections for the target and standard molecules, $S_T(E)$ and $S_S(E)$ are the respective photoionization efficiencies, and P_T and P_S are their partial pressures in the sample mixture. The "mass discrimination factor" $[R_T/R_S]$ for the detection of the target relative to propene is the ratio of the mass-dependent response factors R_T and R_S that account for the respective sampling and detection efficiencies for the target and standard molecules [28,35]. For some target molecules with adiabatic ionization energies lower than that of propene, ion signals, corrected for photon current, are used to extrapolate cross-sections to threshold.

Three binary target/propene sample mixtures are independently prepared for each molecule, with the exception of ketene, for which six samples are prepared, and 3-methyl-1-butene, 2,3-dihydrofuran, and 2,5-dihydrofuran, for which 2 samples are prepared. In addition, samples containing only the target molecule with no admixed propene are studied to determine the dissociative ionization cross-sections. In the case of some molecules, a fragment ion for $m/z = 42$ is observed in the absence of admixed propene. The $m/z = 42$ ion signals for the binary target/propene mixtures are corrected to account for this fragment ion contribution.

The sources of the chemicals used in these studies are as follows: propene 99% (Aldrich), trans-2-butene 99 + % (Aldrich), 2-methyl-1-butene 98% (Aldrich), 3-methyl-1-butene 95% (Aldrich), 2-methyl-2-butene 99+% (Sigma–Aldrich), trans-2-hexene 97% (Aldrich), 1-hexene 99 + % (Aldrich), allene 97% (Aldrich), 1,3-butadiene 99+% (Aldrich), 1,3-pentadiene 98% (Aldrich), 1,4-pentadiene 99% (Aldrich), 3-methyl-1,2-butadiene 97% (Aldrich), 1,5-hexadiene 97% (Aldrich), isobutane 99% (Aldrich), methylcyclohexane 99+% (Sigma–Aldrich), furan 99+% (Aldrich), 2,3-dihydrofuran 99% (Aldrich), 2,5-dihydrofuran 97% (Aldrich), 2-methyltetrahydrofuran 99+% (Sigma–Aldrich), tetrahydropyran 99% (Sigma–Aldrich), butanal 99% (Sigma–Aldrich), isobutanal 99+% (Aldrich), 2-butenal ≥99.5% (Aldrich), 3-methyl-2-butenal 97% (Aldrich), allyl alcohol 98.5+% (Aldrich), methyl vinyl ketone 99% (Aldrich), dimethoxymethane 99% (Sigma–Aldrich), methylamine 99.0+% (Aldrich), ethylamine 99.0% (Aldrich), piperidine 99.0+% (Sigma–Aldrich).

Ketene is not commercially available due to its low boiling point (−59.4 °C) and the tendency to polymerize during long storage periods [46]. We synthesize ketene with the procedures reported by Williams and Hurd [47]. Briefly, 100 ml of acetic anhydride is poured into a round bottomed reaction flask. Dry nitrogen enters the reaction flask through a Teflon tube and passes through the apparatus at a flow rate of approximately 1 bubble per 5 s. The acetic anhydride is heated to its boiling point (138–140 °C) using a heating mantle that is placed beneath the round bottomed flask. When the acetic anhydride begins to reflux, a nichrome coil inserted into the reaction flask is heated until it is observed to be a dull red color. The hot metallic coil cracks the acetic anhydride, and forms gaseous ketene. The gaseous ketene and byproducts travel through a water cooled condenser into a first cold trap. This trap, which is cooled using an ice water bath, catches many impurities such as acetic acid. Ketene exits the first trap and travels through a Teflon tube into a final ketene trap. This trap is cooled to 179 K using a liquid nitrogen/hexane slush that is held in a 1 l dewar. A total of 5 ml of ketene is thus synthesized per experiment. The fresh sample of ketene is stored at −114 °C in a liquid nitrogen/ethanol cooled bubbler. The air in the bubbler is pumped out to yield the pure ketene vapor used to fill the sample cylinders. Nominally 15 Torr ketene, 15 Torr allene and 2300 Torr of argon are combined and allowed to mix for 8 h in a pre-evacuated cylinder before beginning measurements.

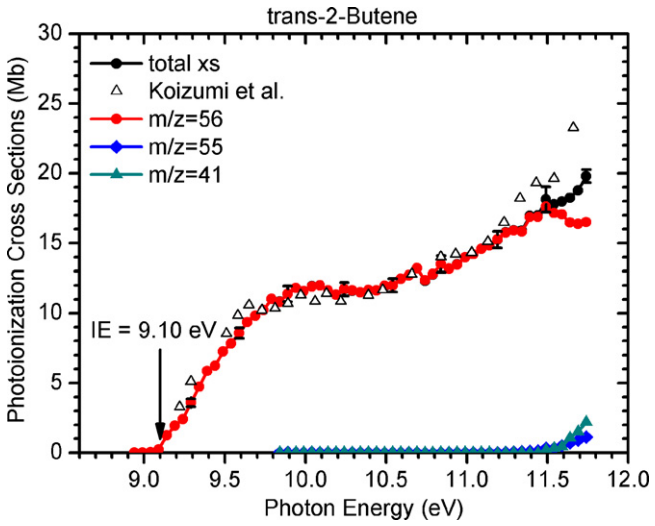

Fig. 1. Molecular and dissociative photoionization cross-sections for trans-2-butene. The total cross-sections are compared with the previous measurements of Koizumi et al. [49,50]. The literature ionization energy (IE) for trans-2-butene [51] is indicated.

3. Results

We present here (Figs. 1–30) near-threshold absolute photoionization and dissociative ionization cross-sections for 30 molecules including alkenes, dienes, alkanes, oxygenates and nitrogenous compounds. As shown with the data for a few representative photon energies, the standard deviations (typically ±10%) for cross-sections determined with separately prepared sample mixtures yield an estimate of the precision of the present measurements. The cross-sections for the propene calibration standard have uncertainties less than ±15%. An overall uncertainty of ±20% is assigned to the cross-sections reported here. The photoionization cross-sections for all the molecules shown below are also given in tabular form in the supplementary data to this paper.

3.1. Trans-2-butene, 2-methyl-1-butene, 3-methyl-1-butene, 2-methyl-2-butene, trans-2-hexene, 1-hexene

The total and mass-resolved partial cross-sections for some monounsaturated alkenes including 1-butene, cis-2-butene,

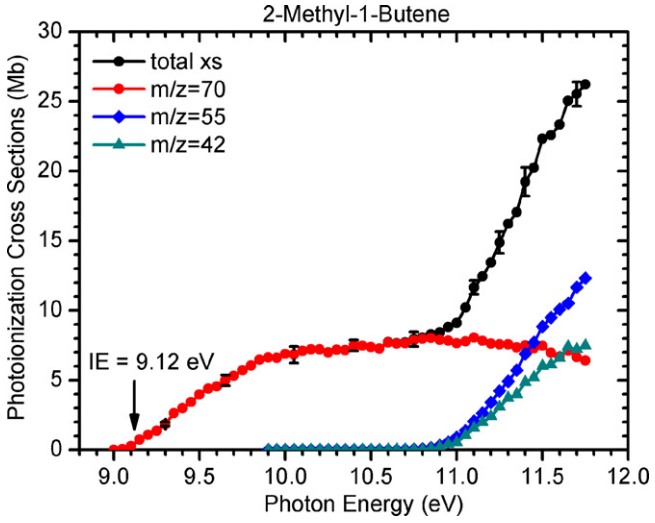

Fig. 2. Molecular and dissociative photoionization cross-sections for 2-methyl-1-butene. The literature IE for 2-methyl-1-butene [51] is indicated.

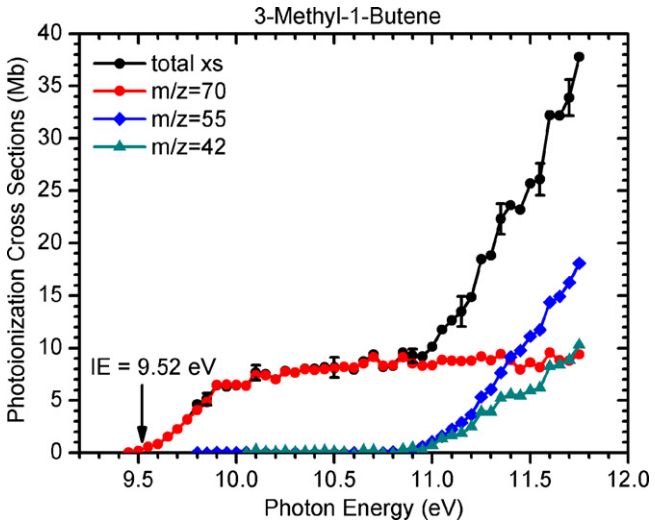

Fig. 3. Molecular and dissociative photoionization cross-sections for 3-methyl-1-butene. The literature IE for 3-methyl-1-butene [51] is indicated.

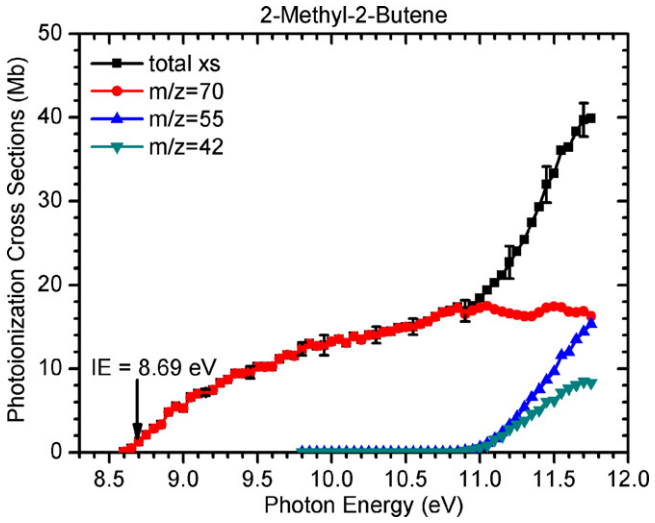

Fig. 4. Molecular and dissociative photoionization cross-sections for 2-methyl-2-butene. The literature IE for 2-methyl-2-butene [51] is indicated.

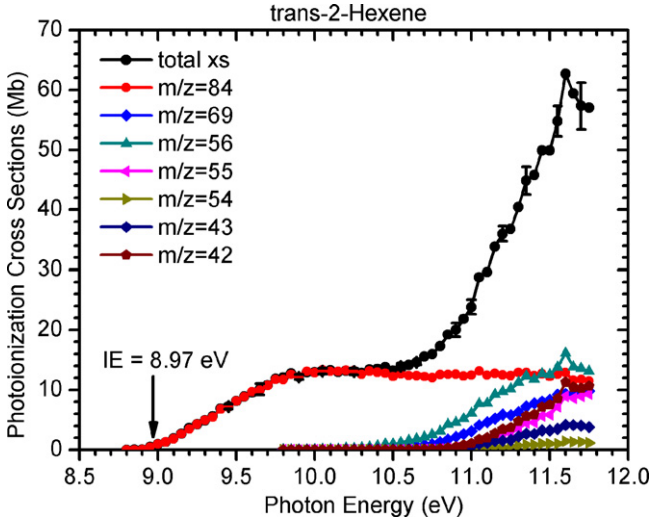

Fig. 5. Molecular and dissociative photoionization cross-sections for trans-2-hexene. The literature IE for trans-2-hexene [51] is indicated.

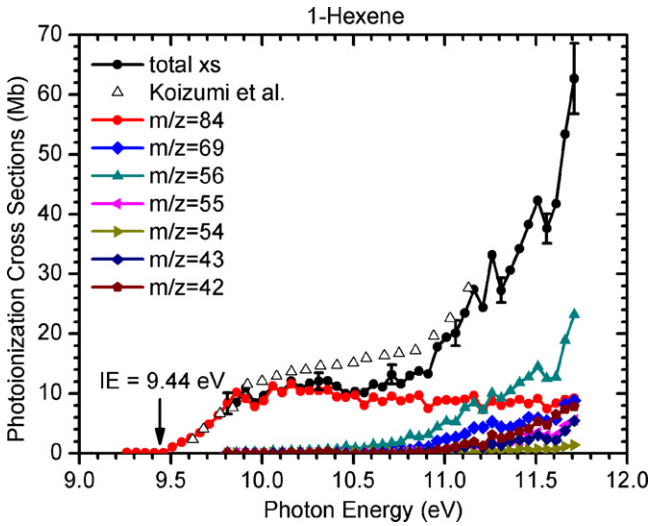

Fig. 6. Molecular and dissociative photoionization cross-sections for 1-hexene. The total cross-sections are compared with the previous measurements of Koizumi et al. [50] The literature IE for 1-hexene [51] is indicated.

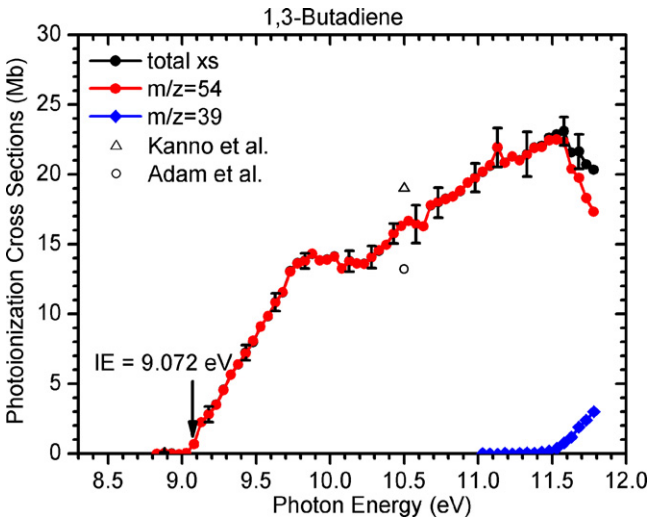

Fig. 8. Molecular and dissociative photoionization cross-sections for 1,3-butadiene. The photoionization cross section at 10.5 eV is compared with the previous measurements of Kanno and Tonokura [34] and Adam and Zimmermann [33]. The literature IE for 1,3-butadiene [51] is indicated.

isobutene, 1-pentene, cis-2-pentene, trans-2-pentene, cyclopentene, cyclohexene and 3,3-dimethylbutene were reported elsewhere [28,35]. The lowest ionization energy for these monounsaturated alkenes corresponds to the removal of an electron from a π orbital of the C=C double bond. The energy separating the first and second ionization energies is often as large as 1–2 eV, which usually leads to a plateau in the PIE curves (PIE *vs* photon energy) just above the threshold, corresponding to photoionization cross-sections of 10–15 Mb. The plateau extends to the second ionization energy of the parent molecule where dissociative ionization channels typically appear. Photoionization cross-sections for another six alkenes are given here, which show similarities with other monounsaturated alkenes.

Fig. 1 shows the mass-resolved photoionization cross-sections for trans-2-butene. Only the parent ion ($m/z = 56$) contributes to the total cross-sections until the opening of dissociative photoionization channels leading to two fragment ions $C_4H_7^+$ ($m/z = 55$) and $C_3H_5^+$ ($m/z = 41$) near the second adiabatic ionization energy for the parent molecule (11.46 eV [48]). As expected the partial cross-sections for trans-2-butene are quantitatively similar to those of

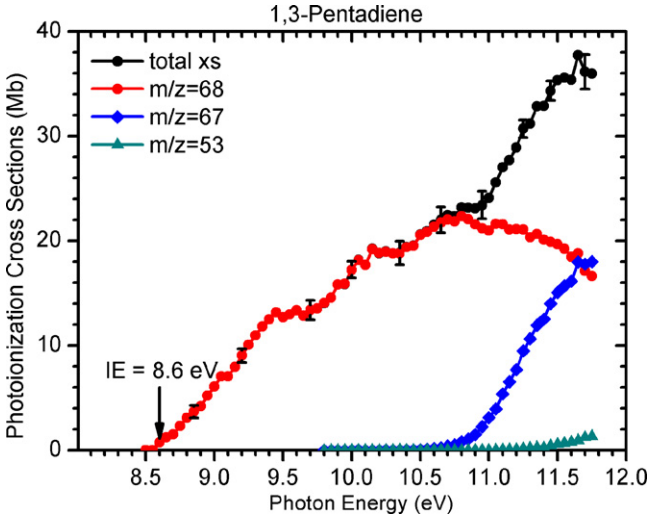

Fig. 9. Molecular and dissociative photoionization cross-sections for 1,3-pentadiene. The literature IE for 1,3-pentadiene [51] is indicated.

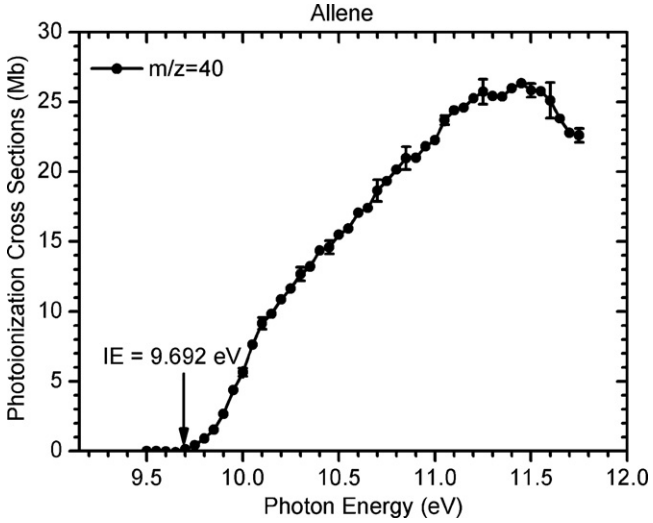

Fig. 7. Molecular and dissociative photoionization cross-sections for allene. The literature IE for allene [51] is indicated.

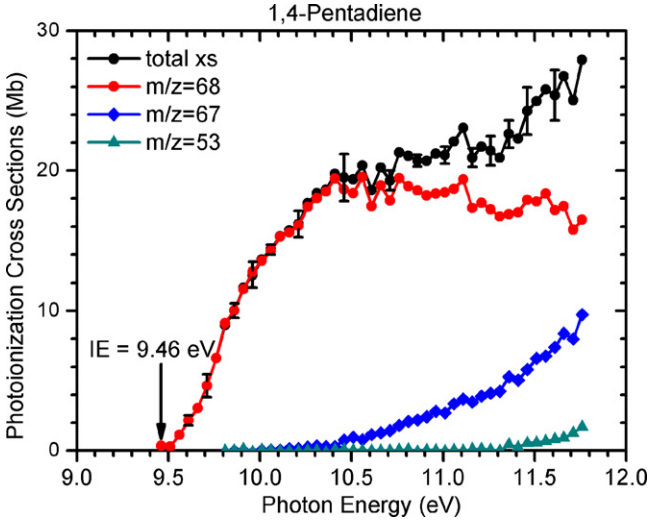

Fig. 10. Molecular and dissociative photoionization cross-sections for 1,4-pentadiene. The literature IE for 1,4-pentadiene [51] is indicated.

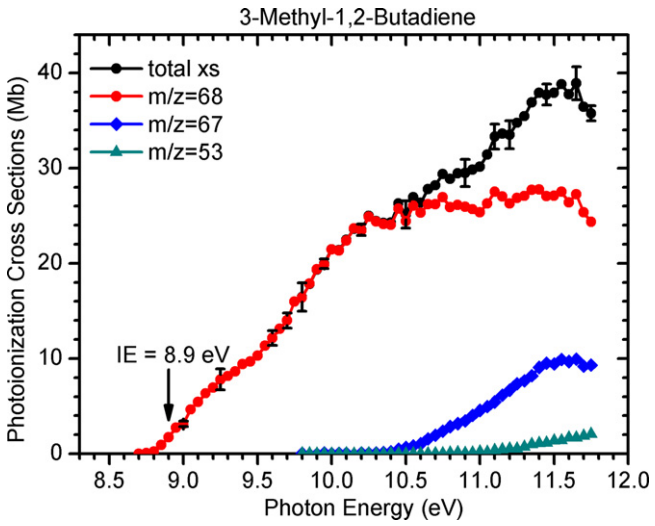

Fig. 11. Molecular and dissociative photoionization cross-sections for 3-methyl-1,2-butadiene. The literature IE for 3-methyl-1,2-butadiene [51] is indicated.

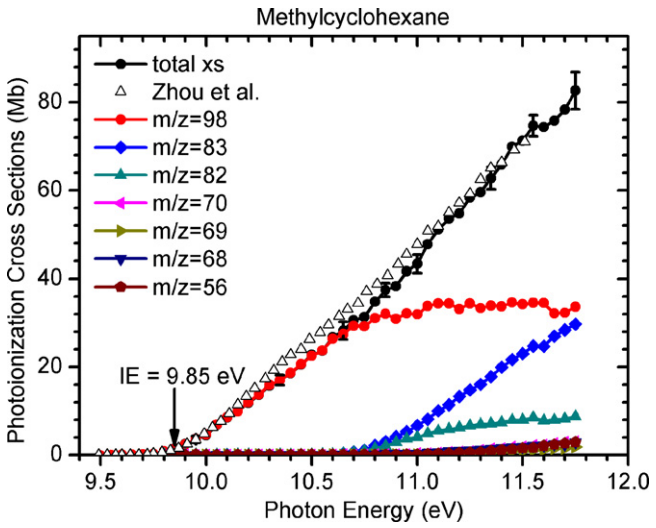

Fig. 14. Molecular and dissociative photoionization cross-sections for methylcyclohexane. The literature IE for methylcyclohexane [51] is indicated.

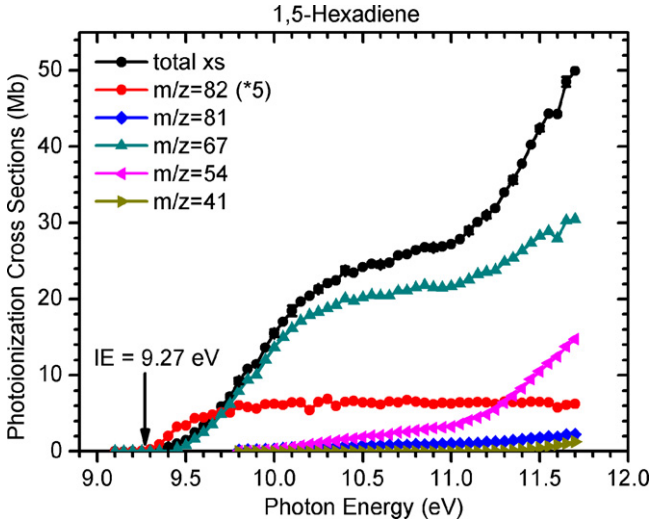

Fig. 12. Molecular and dissociative photoionization cross-sections for 1,5-hexadiene. The literature IE for 1,5-hexadiene [51] is indicated.

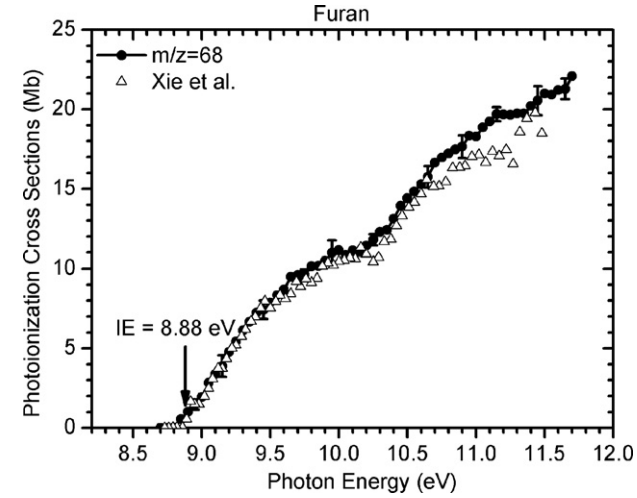

Fig. 15. Molecular and dissociative photoionization cross-sections for furan. The literature IE for furan [51] is indicated.

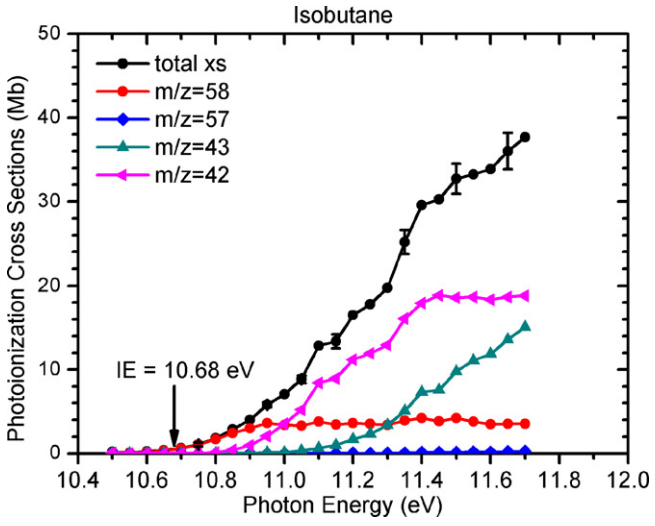

Fig. 13. Molecular and dissociative photoionization cross-sections for isobutane. The literature IE for isobutane [51] is indicated.

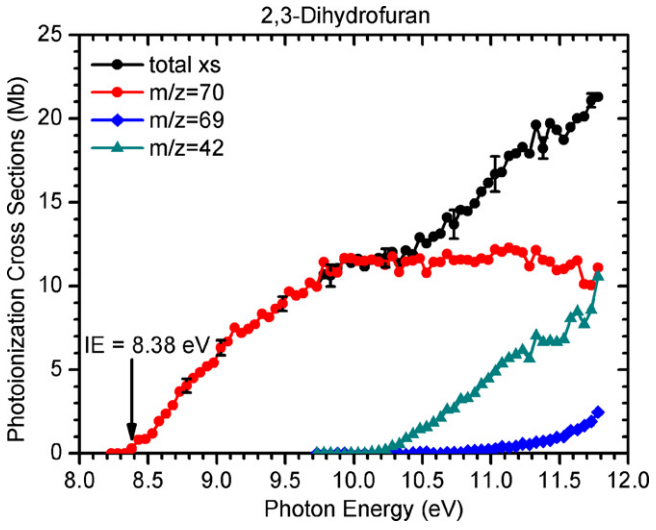

Fig. 16. Molecular and dissociative photoionization cross-sections for 2,3-dihydrofuran. Our measured IE for 2,3-dihydrofuran is indicated.

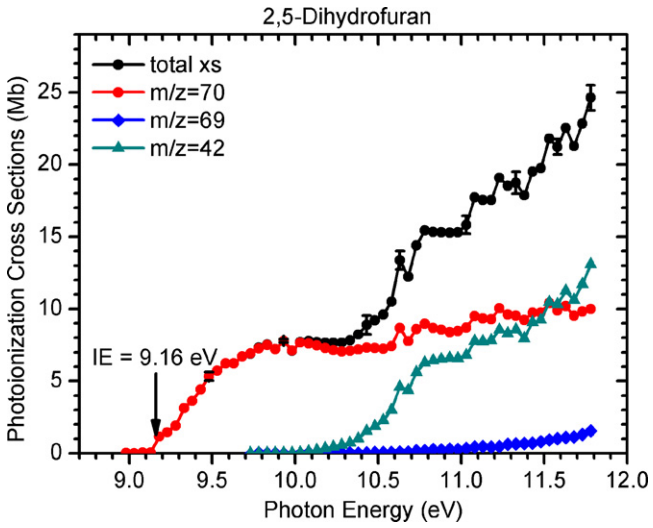

Fig. 17. Molecular and dissociative photoionization cross-sections for 2,5-dihydrofuran. Our measured IE for 2,5-dihydrofuran is indicated.

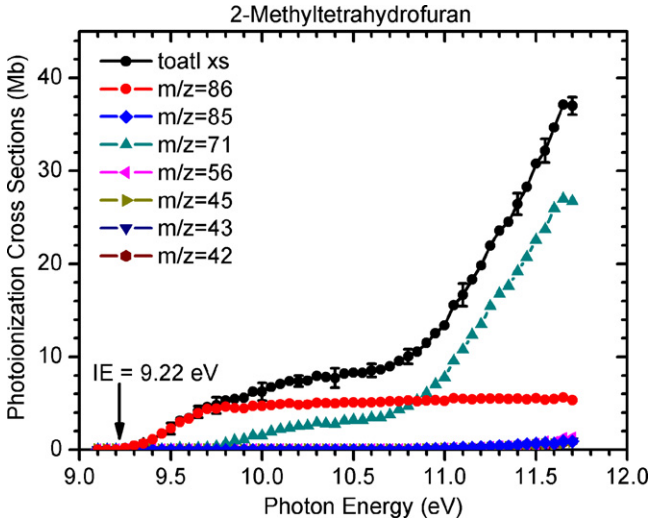

Fig. 18. Molecular and dissociative photoionization cross-sections for 2-methyltetrahydrofuran. The literature IE for 2-methyltetrahydrofuran [51] is indicated.

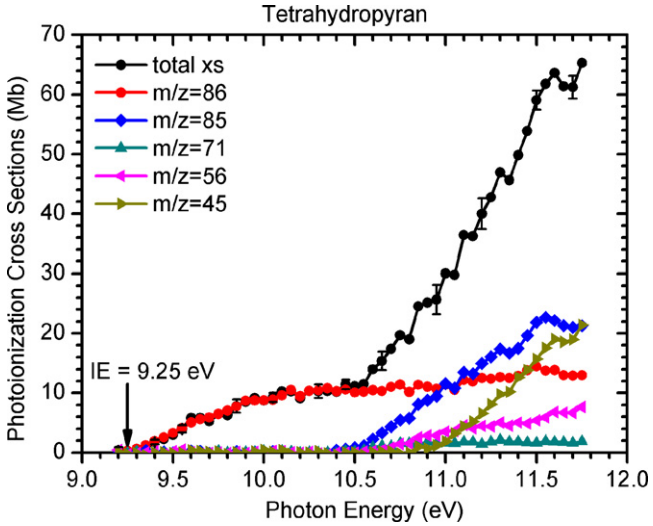

Fig. 19. Molecular and dissociative photoionization cross-sections for tetrahydropyran. The literature IE for tetrahydropyran [51] is indicated.

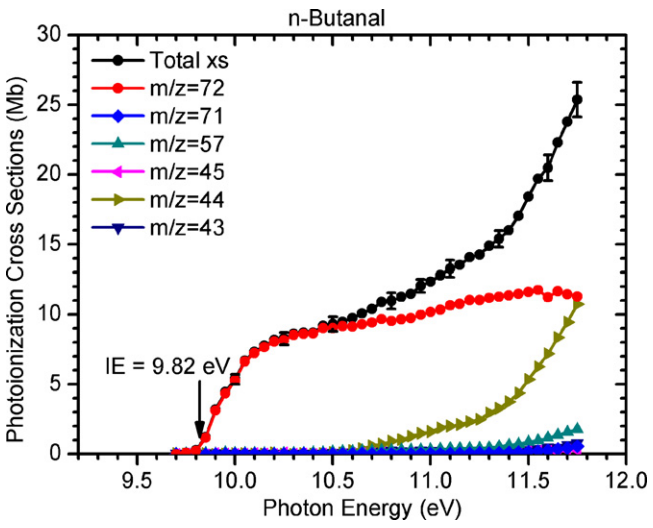

Fig. 20. Molecular and dissociative photoionization cross-sections for n-butanal. The literature IE for n-butanal [51] is indicated.

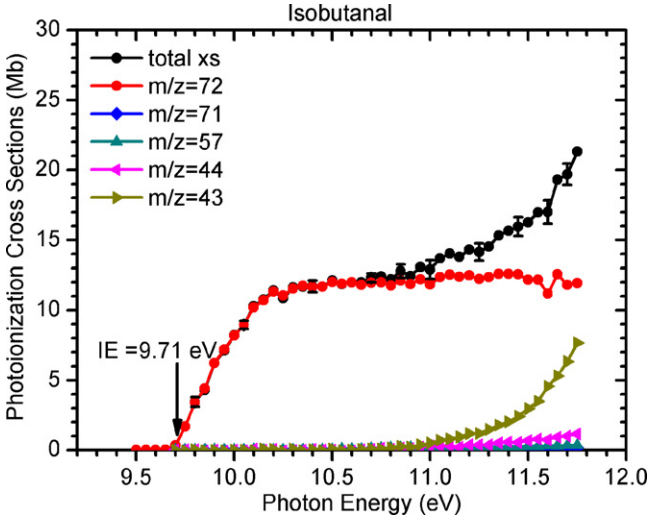

Fig. 21. Molecular and dissociative photoionization cross-sections for isobutanal. The literature IE for isobutanal [51] is indicated.

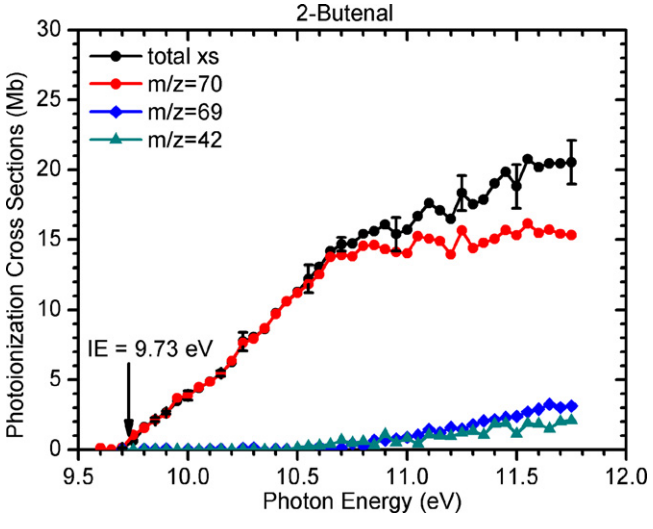

Fig. 22. Molecular and dissociative photoionization cross-sections for 2-butenal. The literature IE for 2-butenal [51] is indicated.

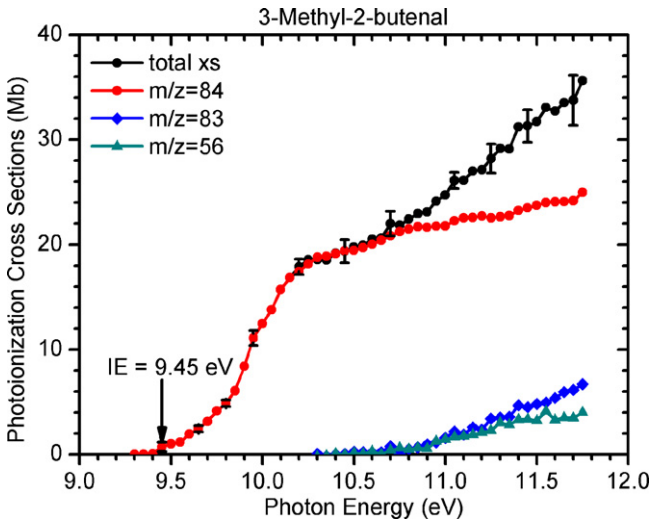

Fig. 23. Molecular and dissociative photoionization cross-sections for 3-methyl-2-butenal. Our measured IE for 3-methyl-2-butenal is indicated.

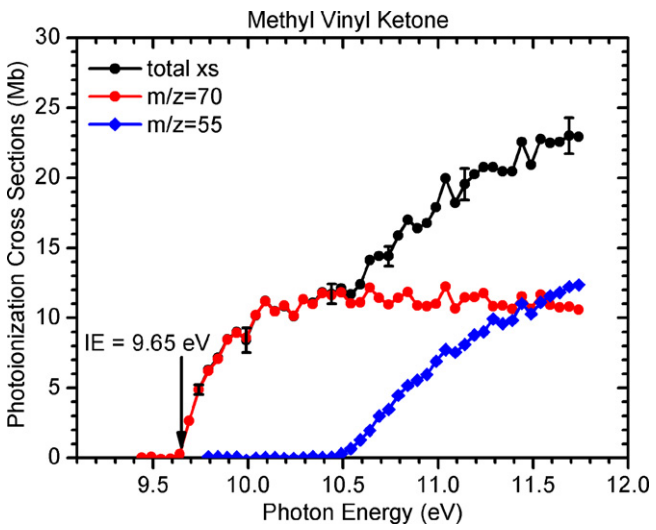

Fig. 26. Molecular and dissociative photoionization cross-sections for methyl vinyl ketone. The literature IE for methyl vinyl ketone [51] is indicated.

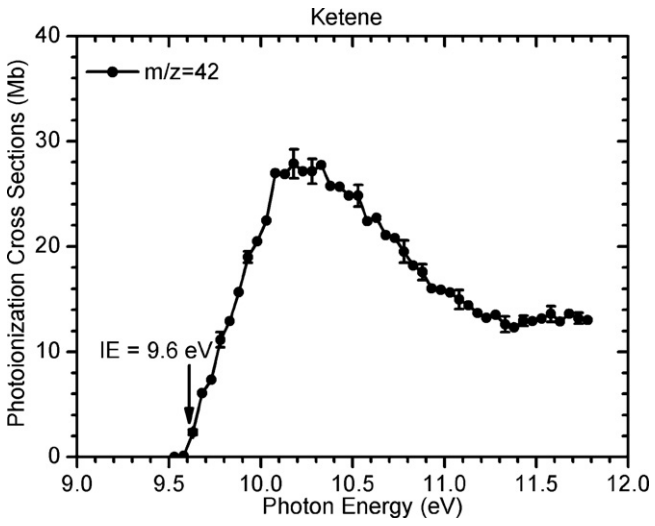

Fig. 24. Molecular and dissociative photoionization cross-sections for ketene. The literature IE for ketene [51] is indicated.

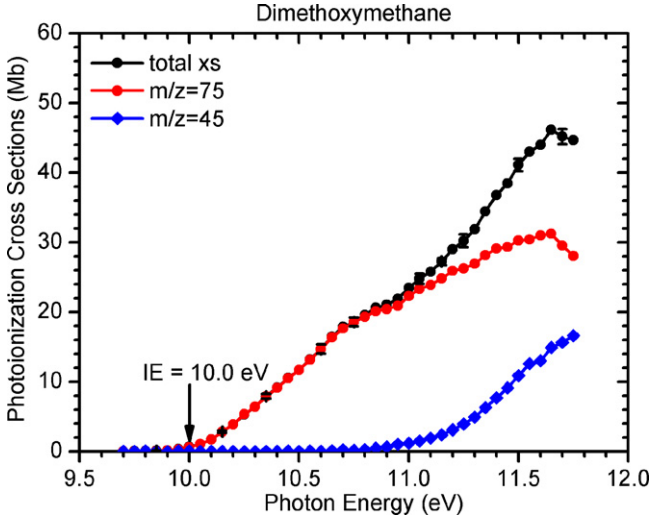

Fig. 27. Molecular and dissociative photoionization cross-sections for dimethoxymethane. The literature IE for dimethoxymethane [51] is indicated.

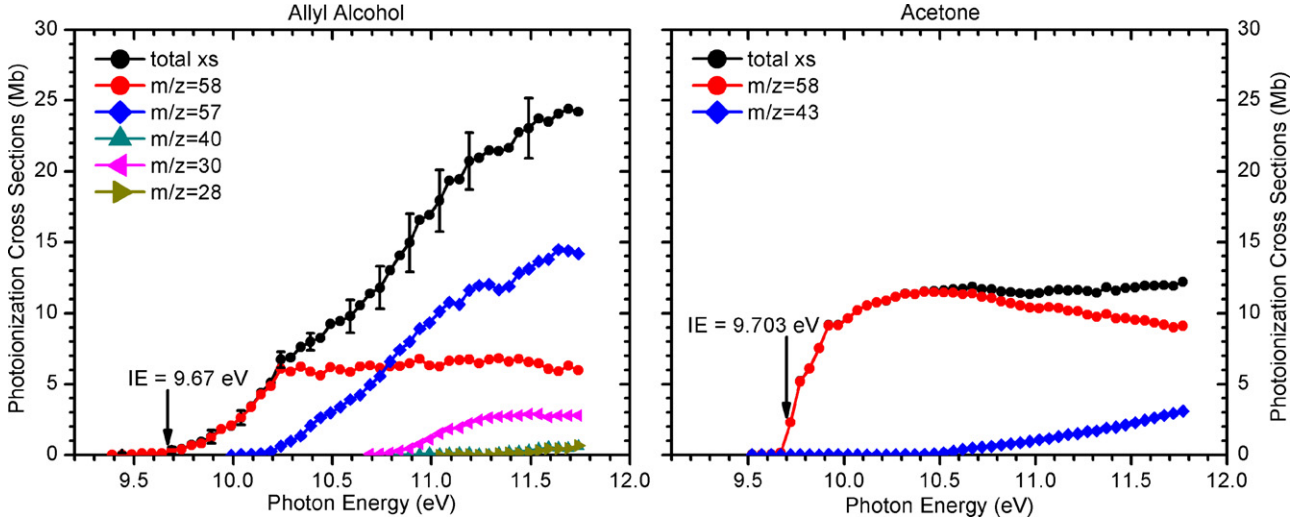

Fig. 25. Molecular and dissociative photoionization cross-sections for allyl alcohol (left). Acetone cross-sections (right) reported previously [35] are also shown for comparison. Their literature IEs [51] are indicated.

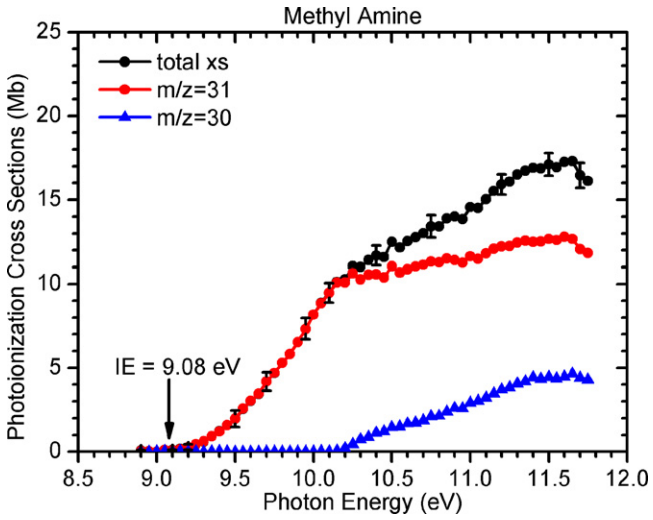

Fig. 28. Molecular and dissociative photoionization cross-sections for methylamine. The literature IE for methylamine [51] is indicated.

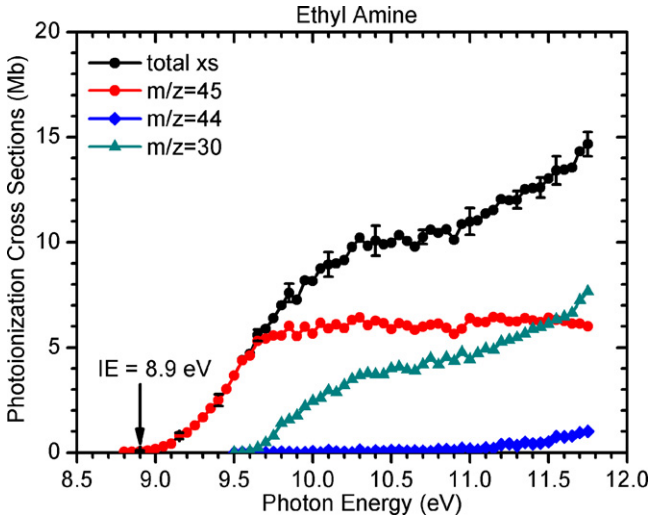

Fig. 29. Molecular and dissociative photoionization cross-sections for ethylamine. The literature IE for ethylamine [51] is indicated.

cis-2-butene [28] due to their similar ionization energies and electron structures. The total cross-sections for trans-2-butene are in good agreement with those reported by Koizumi et al. [49,50]

The molecular and dissociative photoionization cross-sections for 2-methyl-1-butene, 3-methyl-1-butene and 2-methyl-2-butene are presented in Figs. 2–4, respectively. The cross-sections for these three branched alkene isomers with the formula of C_5H_{10} are similar to those of their linear isomers including 1-pentene, cis-2-pentene and trans-2-pentene [28,35]. The parent-ion cross-sections rise smoothly from their respective thresholds to reach plateaus extending to the 11.75 eV limit of the present measurements. Although the IEs for these three isomers are 9.12 eV, 9.52 eV and 8.69 eV [51], respectively, dissociative ionization channels leading to $C_4H_7^+$ (m/z = 55) and $C_3H_6^+$ (m/z = 42) for all three isomers open near 10.8 eV. The contributions from these two fragments make the total cross-sections increase sharply after their appearance. The $C_3H_6^+$ cross-sections required supplementary measurements of the fragmentation of these samples in the absence of admixed propene. No previous cross section measurements for these three isomers have been reported.

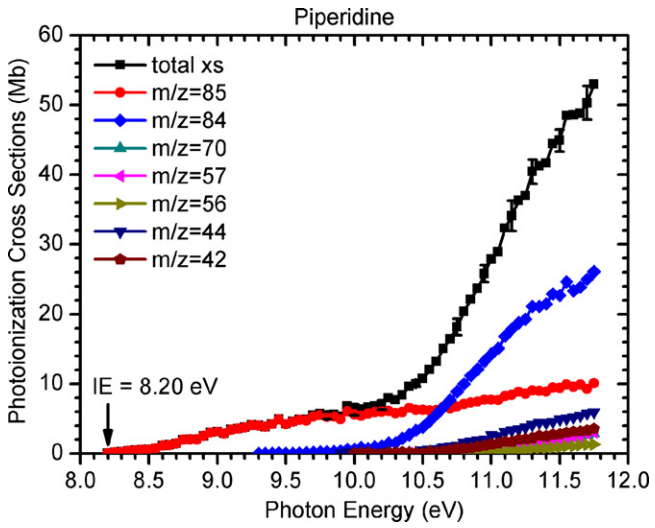

Fig. 30. Molecular and dissociative photoionization cross-sections for piperidine. The literature IE for piperidine [51] is indicated.

Photoionization cross-sections for trans-2-hexene and 1-hexene are shown in Figs. 5 and 6, respectively. Preliminary data for 1-hexene have been given in our previous work [52]. These two isomers exhibit parent ion cross-sections that increase gradually above the thresholds (8.9 and 9.5 eV, respectively) reaching plateaus around 9.8 eV in a fashion typical of other alkenes. The fragment ions $C_5H_9^+$ (m/z = 69), $C_4H_8^+$ (m/z = 56), $C_4H_7^+$ (m/z = 55), $C_4H_6^+$ (m/z = 54), $C_3H_7^+$ (m/z = 43) and $C_3H_6^+$ (m/z = 42) have appearance energies in the 10.5–11.2 eV range [51]. The $C_3H_6^+$ and $C_3H_7^+$ cross-sections require supplementary measurements of the fragmentation of the samples in the absence of admixed propene. The contribution of ^{13}C isotopes of $C_3H_6^+$ is subtracted from the $C_3H_7^+$ (m/z = 43) ion signal. The total cross-sections reported by Koizumi et al. [50] are in reasonable agreement with the present measurement for 1-hexene, while there is no previous report for photoionization cross-sections for trans-2-hexene. As can be seen, various dissociative ionization channels for these two isomers appear only 0.5–1.5 eV above the adiabatic ionization thresholds of the parent molecules. Therefore when these species appear in complex systems such as premixed flames, these dissociative ionization channels must be considered when quantitative information is derived.

3.2. Allene, 1,3-butadiene, 1,3-pentadiene, 1,4-pentadiene, 3-methyl-1,2-butadiene, 1,5-hexadiene

Allene is one of the most important intermediates in hydrocarbon combustion [26] and pyrolysis processes [53]. Accurate cross-sections for allene are desired to enable the measurement of its mole fractions in flames and to determine the relative concentration ratios of allene to its isomer propyne. The cross-sections for allene have thus been reexamined using an apparatus of improved signal/noise ratio [26]. As shown in Fig. 7, the cross section for allene increases smoothly until 11.5 eV and then decreases by about 8% with no observable dissociation channel before 11.75 eV. The higher precision cross-sections for allene reported here are 24% smaller than the values reported previously [3].

A serious anomaly was noted in our previous measurements of cross-sections for 1,3-butadiene [3,34]. Our re-measured absolute photoionization cross-sections for 1, 3-butadiene are presented in Fig. 8. These cross-sections lie between the recent values reported by Kanno and Tonokura [34] and Adam and Zimmermann [33] at 10.5 eV, shown in the figure. Clearly our previous measurements

[3,34] are in error by nearly a factor of 2 as noted in [34]; a discrepancy this large is unprecedented and remains unexplained. The parent ion cross section rises from its threshold at 9.07 eV, reaches a short plateau at 9.8 eV, rises further and then decreases sharply beyond 11.5 eV, where the partial cross section for $C_3H_3^+$ (m/z = 39) begins to contribute to the total cross-sections.

The absolute cross-sections for three isomers of C_5H_8 (1,3-pentadiene, 1,4-pentadiene and 3-methyl-1,2-butadiene) are shown in Figs. 9–11, respectively. The parent cross-sections for all three isomers rise smoothly from their respective thresholds, reach a maximum of around 20 Mb, when competition with the dissociative ionization channels begins, leading to the formation of $C_5H_7^+$ (m/z = 67) and $C_4H_5^+$ (m/z = 53). The shapes for the PIE curves differ somewhat because of their different ionization energies and electron structures.

The absolute cross-sections for 1,5-hexadiene are given in Fig. 12. The parent ion (m/z = 82) cross section, multiplied by a factor of 5 for display, increases slowly from the threshold and reaches a broad plateau near 9.7 eV with a level of less than 1.3 Mb. The partial cross-sections for fragments $C_5H_7^+$ (m/z = 67) with an appearance energy of 9.4 eV contribute most to the total cross-sections while the minor fragment ions $C_6H_9^+$ (m/z = 81), $C_4H_6^+$ (m/z = 54) and $C_3H_5^+$ (m/z = 41) make small contributions below 11.75 eV. It is interesting that the cross-sections for 1,5-hexadiene exhibit totally different features for the parent ion and fragments than those of its isomer 1,3-hexadiene reported previously [28], which may be due to their different electron structures. However, the near-threshold total cross-sections for these two isomers are quite similar. No previous cross section measurements are available for 1,5-hexadiene.

3.3. Isobutane, methylcyclohexane

The absolute cross-sections for isobutane are shown in Fig. 13. The total cross section rises monotonically above the threshold until 11.7 eV, which is comparable with that of n-butane, reported previously [28]. Although both n-butane and isobutane have similar ionization energies and appearance energies for fragments $C_3H_7^+$ (m/z = 43) and $C_3H_6^+$ (m/z = 42), the relative contributions from parent and fragment ions to the total cross-sections are different. For example, the parent ion of isobutane makes a much smaller contribution to the total cross section compared with that of the parent ion of n-butane. The $C_3H_6^+$ cross-sections require supplementary measurements of the fragmentation of isobutane in the absence of admixed propene.

Fig. 14 presents the molecular and dissociative photoionization cross-sections for methylcyclohexane. As can be seen, the total cross-sections are in good agreement with the values reported by Zhou et al. [30]. Their measurements were performed with a photoionization mass spectrometer with a binary-liquid-mixture method utilizing benzene as a calibration standard for the photon energy range from the ionization threshold to 11.5 eV. The total cross section rises monotonically above the threshold in a quasi-linear fashion in agreement with previously reported near thresholds cross-sections for alkanes [28,54]. Several photodissociation channels open around 10.7 eV, competing with the parent ion. Compared with the work of Zhou et al. [30], two more fragment ions $C_5H_9^+$ (m/z = 69) and $C_5H_8^+$ (m/z = 68) are observed, although their contributions to the total cross-sections are smaller than the major fragments of $C_6H_{11}^+$ (m/z = 83) and $C_6H_{10}^+$ (m/z = 82).

3.4. Oxygenates

Increasing attention has been paid to the renewable and environmentally friendly biofuels, and PIMS is widely used for the study of the oxidation of oxygenated compounds [55]. Mass-resolved partial cross-sections for more oxygenates are highly desired to supplement previously reported cross-sections for some alcohols [28,31,35], ethers [31,35], esters [27,28], aldehydes [26,28] and fatty acids [35]. Molecular and dissociative photoionization cross-sections for thirteen oxygenates including cyclo ethers, aldehydes and ketene are given below.

3.4.1. Furan, 2,3-dihydrofuran, 2,5-dihydrofuran, 2-methyl-tetrahydrofuran, tetrahydropyran

The absolute cross-sections for furan are shown in Fig. 15, which are in good agreement with the measurements of Xie et al. [31]. Their measurements were performed with PIMS using the above mentioned binary-liquid-mixture method utilizing acetone as a calibration standard for the photon energy range from the ionization threshold to 11.5 eV. In agreement with the results of Xie et al. no fragment contributes to the total cross section at energies below 11.75 eV.

Figs. 16 and 17 display the cross-sections for 2,3-dihydrofuran and 2,5-dihydrofuan. For both molecules the parent ion cross-sections rise from the ionization thresholds slowly and reach an extensive plateau around 10.0 eV, although their ionization energies differ by about 0.7 eV. Similar dissociation channels leading to the fragments of $C_4H_5O^+$ (m/z = 69) and $C_2H_2O^+$ (m/z = 42) contribute to the total cross-sections with similar appearance energies of 10.3 and 10.7 eV, respectively. The accurate determination of the $C_2H_2O^+$ cross-sections requires supplementary measurements of the fragmentation of these samples in the absence of admixed propene. No previous cross section measurements for both isomers have been reported.

The 2-methyltetrahydrofuran photoionization cross-sections for parent $C_5H_{10}O^+$ (m/z = 86), predominant fragment $C_4H_7O^+$ (m/z = 71) and other minor fragments are shown in Fig. 18. The parent ion cross section rises from threshold at 9.2 eV [51] to reach a plateau before the onset of dissociative ionization near 9.7 eV, extending to the limit of the present measurements. The $C_4H_7O^+$ fragment appears only 0.3 eV above the parent ionization energy, corresponding to loss of the branched CH_3 group from the parent ion. The $C_4H_7O^+$ fragment ion and total ionization cross-sections rise steeply beyond 10.8 eV, where the five-atom ring of the parent ion may open, leading to other dissociation channels for $C_4H_7O^+$ and other minor fragments.

Compared with the 2-methyltetrahydrofuran, tetrahydropyran consists of a six-atom ring and the mass-resolved partial cross-sections show different features (Fig. 19). For example, the parent ion cross-sections for tetrahydropyran are higher than those for 2-methyltetrahydrofuran, and the fragment ion $C_5H_9O^+$ (m/z = 85) for tetrahydropyran contributes more to the total cross-sections than it does for 2-methyltetrahydrofuran. The fragment ion $C_4H_7O^+$ (m/z = 71) appears 1.5 eV above the ionization threshold, where the six-atom ring for the parent ion is open leading to the formations of several other fragment ions. From these results, the mass selected partial cross-sections are clearly highly affected by the molecular structures.

3.4.2. Butanal, isobutanal, 2-butenal, 3-methyl-2-butenal

Photoionization cross section *vs* energy profiles for n-butanal and isobutanal presented in Figs. 20 and 21 show trends similar to those seen in the previously published photoionization cross-sections for acetaldehyde [26] and propanal [28]. The ionization energies of these simple aldehydes correspond to the removal of a nonbonding electron from the carbonyl oxygen. The parent ion cross-sections for both n-butanal and isobutanal rise smoothly from their respective ionization energies to reach plateaus of similar shape and magnitude to those observed for acetaldehyde and propanal [26,28]. However, more dissociation channels for these two C_4 aldehydes make contributions to the total cross-sections

before the energy cutoff of the current measurements, as shown in the figures. It should be pointed out that $C_2H_4O^+$ (m/z = 44) with appearance energy of 10.52 eV [51] is the predominant fragment ion for n-butanal, while $C_2H_3O^+$ (m/z = 43) with appearance energy of 10.90 eV is the dominant fragment ion for isobutanal, reflecting differences in their $C_4H_7^\bullet$ structures.

Photoionization cross-sections for two unsaturated aldehydes 2-butenal and 3-methyl-2-butenal are shown in Figs. 22 and 23. 2-Butenal, usually called crotonaldehyde (C_4H_6O) is an isomer of 2,3-dihydrofuran and 2,5-dihydrofuran. All these three isomers produce fragment ions with m/z = 69 and m/z = 42 at energies below 11.75 eV. However, $C_3H_6^+$ is likely the m/z = 42 fragment for 2-butenal with an appearance energy of 10.5 eV, while $C_2H_2O^+$ is the m/z = 42 fragment for dihydrofuran isomers with an appearance energy of 10.2 eV. The m/z = 42 cross-sections require supplementary measurements of the fragmentation of 2-butenal in the absence of admixed propene. 3-Methyl-2-butenal, also called β-methylcrotonaldehyde, shows a fragment cross section *vs* energy profile similar to that of 2-butenal, as seen in Fig. 24. Fragment ions for both molecules are formed through loss of an H-atom or CO from respective parent ions during the ionization process. No previous cross section measurements for 2-butenal and 3-methyl-2-butenal have been reported.

3.4.3. Ketene, allyl alcohol, methylvinylketone, dimethyoxymethane

Ketene is a very important combustion intermediate of particular importance in biofuel combustion [55,56], so the determination of its absolute photoionization cross section is highly desirable. Due to its high reactivity at room temperature, the photoionization cross section of this important intermediate has until now not been measured. Because both ketene and propene have the same m/z, it is not possible to use propene as the standard at the resolution of our mass spectrometer. The well measured cross-sections for allene, shown in Fig. 7, are used as the standard in this study. Six separately prepared sample mixtures of ketene and allene are measured and the average cross-sections and standard deviations are shown in Fig. 24. No fragment ion is observed below 11.75 eV. The shape of the cross section *vs* energy profile for ketene differs greatly from that of propene, which provides an opportunity to compare flame-sampled PIE curves for m/z = 42 with the known cross-sections of ketene and propene to identify and quantify these two species in flames [56].

Ally alcohol is an isomer of acetone with almost the same ionization energy (9.67 and 9.70 eV, respectively [51]). It is not easy to distinguish these two isomers without knowing their respective cross-sections [9]. Fig. 25 (left) shows the cross-sections for allyl alcohol. The parent ion cross section rises slowly and reaches a broad plateau at about 10.2 eV, where the dissociation channel to $C_3H_5O^+$ (m/z = 57) starts competing with the parent ion and then 3 more fragments appear before 11.75 eV. The total cross section rises monotonically in a quasi-linear fashion similar to typical cross-sections for alkanes. These cross section features do not appear for acetone [35].

Fig. 26 presents the cross-sections for methyl vinyl ketone (C_4H_6O). The parent ion cross section exhibits a behavior similar to that of other oxygenated compounds. The fragment $C_3H_3O^+$, with an appearance of 10.5 eV, is formed by losing a CH_3 from the parent ion. A similar fragmentation process occurs in acetone [35]. Because methyl radical and vinyl radical can be easily produced through laser photolysis of methyl vinyl ketone, the cross-sections for these radicals can be measured accurately if the cross-sections for methyl vinyl ketone are known [37].

Fig. 27 shows the cross section for dimethoxymethane ($C_3H_8O_2$). It is interesting that the parent ion is not observed, and the fragment ion $C_3H_7O^+$ formed through H-atom loss from the parent ion dominates the total cross-sections below 11.75 eV. Another fragment $C_2H_5O^+$ (m/z = 45), which is formed through the loss of CH_3O, contributes to the total cross-sections above 10.9 eV.

3.5. Methylamine, ethylamine, piperidine

The photoionization cross-sections for isomers of propylamine and butylamine have been measured with PIMS using binary-liquid-mixtures of target and standard species [32]. Photoionization cross-sections for two simpler amines, methylamine and ethylamine, have, until now, not been measured. Figs. 28 and 29 show these cross-sections. The lowest ionization energies for these amines correspond to the loss of an electron from the nitrogen lone electron pair. As a result and because of their similar molecular structures, the ionization energies for all these amines are near 9.1 eV. For methylamine, a fragment CH_4N^+ (m/z = 30) appears at 10.2 eV, which is in good agreement with the data reported by Lossing et al. [57]. For ethylamine, two fragment ions $C_2H_6N^+$ (m/z = 44) and CH_4N^+ (m/z = 30) are formed by losing a H-atom or CH_3 from the parent ion with appearance energies of 11.1 eV and 9.65 eV, respectively [57].

Fig. 30 shows the total and mass-selected partial photoionization cross-sections for piperidine ($C_5H_{11}N$). The parent ion cross section increases slowly from the threshold at 8.2 eV until 11.75 eV, while the total cross section rises sharply when several photodissociation channels including one leading to the dominant fragment $C_5H_{10}N^+$ (m/z = 84) open after 10.4 eV.

It is interesting to compare the cross-sections for piperidine with tetrahydropyran (Fig. 19), both with six-membered ring containing five methylene units and one nitrogen atom *vs* one oxygen atom. Similar trends are observed for the total cross-sections, parent ion cross-sections and the dominant fragment m/z = 85 cross-sections, however, more dissociation channels are observed for piperidine, which is due to the fact the cutoff energy 11.75 eV for current measurements is more than 3.5 eV higher than the ionization threshold for piperidine while only 2.5 eV higher for tetrahydropyran.

4. Conclusions

Experimental measurements of the absolute total and mass-selected partial photoionization cross-sections for 30 combustion intermediates have been performed with tunable synchrotron VUV photoionization mass spectrometry using the well measured propene as a standard. Photoionization cross-sections for six alkenes show similar features to those for other alkenes reported previously, i.e., a typical plateau on the total cross section PIE curves exists due to the large gap between the first and second ionization energies. Photoionization cross-sections for six dienes including allene, 1,3-butadiene, 1,3-pentadiene, 1,4-pentadiene, 3-methyl-1,2-butadiene, 1,5-hexadiene significantly increase the number of available cross-sections for diene species. Photoionization cross-sections for thirteen oxygenates including furan, 2,3-dihydrofuran, 2,5-dihydrofuran, 2-methyltetrahydrofuran, tetrahydropyran, n-butanal, isobutanal, 2-butenal, 3-methyl-2-butenal, ketene, allyl alcohol, methyl vinyl ketone, and dimethoxymethane enrich the pool of photoionization cross sections for biofuel combustion intermediates. And finally, photoionization cross-sections for three nitrogenous compounds including methylamine, ethylamine and piperidine are reported for the first time. The photoionization cross-sections presented here, along with those previously published, increase the utility of single-photon ionization mass spectrometry for studies of combustion chemistry.

Acknowledgements

The authors are grateful to Paul Fugazzi and Sarah Ferrell for expert technical assistance. We thank Tina Kasper, Patrick Oßwald, and Wenjun Li for experimental assistance. This work is supported by the Division of Chemical Sciences, Geosciences, and Biosciences, the Office of Basic Energy Sciences, the U.S. Department of Energy, in part under grant DE-FG02-01ER15180. Sandia is a multi-program laboratory operated by Sandia Corporation, a Lockheed Martin Company, for the National Nuclear Security Administration under contract DE-AC04-94-AL85000. The Advanced Light Source is supported by the Director, Office of Science, Office of Basic Energy Sciences, Materials Sciences Division, of the U.S. Department of Energy under Contract No. DE-AC02-05CH11231 at Lawrence Berkeley National Laboratory.

Appendix A. Supplementary data

Supplementary data associated with this article can be found, in the online version, at doi:10.1016/j.ijms.2011.09.006.

References

[1] B. Oktem, M.P. Tolocka, M.V. Johnston, Anal. Chem. 76 (2004) 253–261.
[2] C.A. Taatjes, J. Phys. Chem. A 110 (2006) 4299–4312.
[3] T.A. Cool, K. Nakajima, T.A. Mostefaoui, F. Qi, A. McIlroy, P.R. Westmoreland, M.E. Law, L. Poisson, D.S. Peterka, M. Ahmed, J. Chem. Phys. 119 (2003) 8356–8365.
[4] Y.Y. Li, F. Qi, Acc. Chem. Res. 43 (2010) 68–78.
[5] N. Hansen, T.A. Cool, P.R. Westmoreland, K. Kohse-Hoinghaus, Prog. Energy Combust. 35 (2009) 168–191.
[6] E.R. Mysak, K.R. Wilson, M. Jimenez-Cruz, M. Ahmed, T. Baer, Anal. Chem. 77 (2005) 5953–5960.
[7] G. Meloni, T.M. Selby, F. Goulay, S.R. Leone, D.L. Osborn, C.A. Taatjes, J. Am. Chem. Soc. 129 (2007) 14019–14025.
[8] N. Hansen, S.J. Klippenstein, C.A. Taatjes, J.A. Miller, J. Wang, T.A. Cool, B. Yang, R. Yang, L.X. Wei, C.Q. Huang, J. Wang, F. Qi, M.E. Law, P.R. Westmoreland, J. Phys. Chem. A 110 (2006) 3670–3678.
[9] B. Yang, P. Osswald, Y.Y. Li, J. Wang, L.X. Wei, Z.Y. Tian, F. Qi, K. Kohse-Hoinghaus, Combust. Flame 148 (2007) 198–209.
[10] T.A. Cool, K. Nakajima, C.A. Taatjes, A. McIlroy, P.R. Westmoreland, M.E. Law, A. Morel, Proc. Combust. Inst. 30 (2005) 1681–1688.
[11] J.C. Person, J. Chem. Phys. 43 (1965) 2553–2555.
[12] J.C. Person, P.P. Nicole, J. Chem. Phys. 49 (1968) 5421.
[13] J.C. Person, P.P. Nicole, J. Chem. Phys. 53 (1970) 1767.
[14] J.C. Person, P.P. Nicole, J. Chem. Phys. 55 (1971) 3390.
[15] K. Kameta, M. Ukai, N. Terazawa, K. Nagano, Y. Chikahiro, N. Kouchi, Y. Hatano, K. Tanaka, AIP Conf. Proc. 258 (1992) 92–99.
[16] K. Kameta, M. Ukai, N. Terazawa, K. Nagano, Y. Chikahiro, N. Kouchi, Y. Hatano, K. Tanaka, J. Chem. Phys. 95 (1991) 6188–6189.
[17] K. Kameta, M. Ukai, T. Numazawa, N. Terazawa, Y. Chikahiro, N. Kouchi, Y. Hatano, K. Tanaka, J. Chem. Phys. 99 (1993) 2487–2494.
[18] K. Kameta, M. Ukai, T. Kamosaki, K. Shinsaka, N. Kouchi, Y. Hatano, K. Tanaka, J. Chem. Phys. 96 (1992) 4911–4917.
[19] K. Kameta, M. Ukai, R. Chiba, K. Nagano, N. Kouchi, Y. Hatano, K. Tanaka, J. Chem. Phys. 95 (1991) 1456–1460.
[20] K. Kameta, T. Seta, M. Watanabe, N. Kouchi, Y. Hatano, J. Electron. Spectrosc. 103 (1999) 65–68.
[21] K. Kameta, K. Muramatsu, S. Machida, N. Kouchi, Y. Hatano, J. Phys. B: Atom. Mol. Opt. 32 (1999) 2719–2728.
[22] K. Kameta, S. Machida, M. Kitajima, M. Ukai, N. Kouchi, Y. Hatano, K. Ito, J. Electron. Spectrosc. 79 (1996) 391–393.
[23] K. Kameta, N. Kouchi, M. Ukai, Y. Hatano, J. Electron. Spectrosc. 123 (2002) 225–238.
[24] D.M.P. Holland, D.A. Shaw, A. Hopkirk, M.A. Macdonald, S.M. Mcsweeney, J. Phys. B: Atom. Mol. Opt. 25 (1992) 4823–4834.
[25] D.A. Shaw, D.M.P. Holland, M.A. Macdonald, A. Hopkirk, M.A. Hayes, S.M. Mcsweeney, Chem. Phys. 166 (1992) 379–391.
[26] T.A. Cool, A. McIlroy, F. Qi, P.R. Westmoreland, L. Poisson, D.S. Peterka, M. Ahmed, Rev. Sci. Instrum. 76 (2005) 094102.
[27] J. Wang, B. Yang, T.A. Cool, N. Hansen, Int. J. Mass Spectrom. 292 (2010) 14–22.
[28] J. Wang, B. Yang, T.A. Cool, N. Hansen, T. Kasper, Int. J. Mass Spectrom. 269 (2008) 210–220.
[29] Z. Zhou, M. Xie, Z. Wang, F. Qi, Rapid Commun. Mass Spectrom. 23 (2009) 3994–4002.
[30] Z. Zhou, L. Zhang, M. Xie, Z. Wang, D. Chen, F. Qi, Rapid Commun. Mass Spectrom. 24 (2010) 1335–1342.
[31] M. Xie, Z. Zhou, Z. Wang, D. Chen, F. Qi, Int. J. Mass Spectrom. 293 (2010) 28–33.
[32] M. Xie, Z. Zhou, Z. Wang, D. Chen, F. Qi, Int. J. Mass Spectrom. 13 (2011) 137–146.
[33] T. Adam, R. Zimmermann, Anal. Bioanal. Chem. 389 (2007) 1941–1951.
[34] N. Kanno, K. Tonokura, Appl. Spectrosc. 61 (2007) 896–902.
[35] T.A. Cool, J. Wang, K. Nakajima, C.A. Taatjes, A. McIlroy, Int. J. Mass Spectrom. 247 (2005) 18–27.
[36] J.C. Loison, J. Phys. Chem. A 114 (2010) 6515–6520.
[37] C.A. Taatjes, D.L. Osborn, T.M. Selby, G. Meloni, H.Y. Fan, S.T. Pratt, J. Phys. Chem. A 112 (2008) 9336–9343.
[38] B.L. FitzPatrick, M. Maienschein-Cline, L.J. Butler, S.-H. Lee, J.J. Lin, J. Phys. Chem. A 111 (2007) 12417–12422.
[39] J.C. Robinson, N.E. Sveum, D.M. Neumark, J. Chem. Phys. 119 (2003) 5311–5314.
[40] J.C. Robinson, N.E. Sveum, D.M. Neumark, Chem. Phys. Lett. 383 (2004) 601–605.
[41] H. Fan, L.B. Harding, S.T. Pratt, Mol. Phys. 105 (2007) 1517–1534.
[42] H. Fan, S.T. Pratt, J. Chem. Phys. 124 (2006) 114312.
[43] N.E. Sveum, S.J. Goncher, D.M. Neumark, Phys. Chem. Chem. Phys. 8 (2006) 592–598.
[44] V.A. Shubert, S.T. Pratt, J. Phys. Chem. A 114 (2010) 11238–11243.
[45] P.A. Heimann, M. Koike, C.W. Hsu, D. Blank, X.M. Yang, A.G. Suits, Y.T. Lee, M. Evans, C.Y. Ng, C. Flaim, H.A. Padmore, Rev. Sci. Instrum. 68 (1997) 1945–1951.
[46] S. Andreades, H.D. Carlson, Org. Synth. Coll. 5 (1973) 679.
[47] J.W. Williams, C.D. Hurd, J. Org. Chem. 5 (1940) 122–125.
[48] M.J.S. Dewar, S.D. Worley, J. Chem. Phys. 50 (1969) 654.
[49] H. Koizumi, T. Yoshimi, K. Shinsaka, M. Ukai, M. Morita, Y. Hatano, A. Yagishita, K. Ito, J. Chem. Phys. 82 (1985) 4856–4861.
[50] H. Koizumi, K. Shinsaka, T. Yoshimi, K. Hironaka, S. Arai, M. Ukai, M. Morita, H. Nakazawa, A. Kimura, Y. Hatano, Y. Ito, Y. Zhang, A. Yagishita, K. Ito, K. Tanaka, Radiat. Phys. Chem. 32 (1988) 111–115.
[51] P.J. Linstrom, W.G. Mallard (Eds.), NIST Chemistry WebBook, NIST Standard Reference Database Number 69, National Institute of Standards and Technology, Gaithersburg MD, 20899, http://webbook.nist.gov.
[52] N. Hansen, W. Li, M.E. Law, T. Kasper, P.R. Westmoreland, B. Yang, T.A. Cool, A. Lucassen, Phys. Chem. Chem. Phys. 12 (2010) 12112–12122.
[53] T. Yuan, L.D. Zhang, Z.Y. Zhou, M.F. Xie, L.L. Ye, F. Qi, J. Phys. Chem. A 115 (2011) 1593–1601.
[54] H. Koizumi, J. Chem. Phys. 95 (1991) 5846–5852.
[55] K. Kohse-Hoinghaus, P. Osswald, T.A. Cool, T. Kasper, N. Hansen, F. Qi, C.K. Westbrook, P.R. Westmoreland, Angew. Chem. Int. Ed. 49 (2010) 3572–3597.
[56] B. Yang, C.K. Westbrook, T.A. Cool, N. Hansen, K. Kohse-Hoinghaus, Phys. Chem. Chem. Phys. 13 (2011) 7205–7217.
[57] F.P. Lossing, Y.T. Lam, A. Maccoll, Can. J. Chem. 59 (1981) 2228–2231.